

Propagation-enhanced generation of intense high-harmonic continua in the 100-eV spectral region: supplementary material

D. E. RIVAS^{1,2,11,12,†}, B. MAJOR^{3,4,†}, M. WEIDMAN¹, W. HELML^{2,5},
G. MARCUS^{1,6}, R. KIENBERGER^{1,5}, D. CHARALAMBIDIS^{4,7,8}, P. TZALLAS^{4,7},
E. BALOGH³, K. KOVÁCS⁹, V. TOSA⁹, B. BERGUES^{1,2}, K. VARJÚ^{3,4} AND L. VEISZ^{1,10,*}

¹Max-Planck-Institut für Quantenoptik, Hans-Kopfermann Strasse 1, 85748, Garching, Germany

²Fakultät für Physik, Ludwig-Maximilians-Universität München, Am Coulombwall 1, 85748 Garching, Germany

³Department of Optics and Quantum Electronics, University of Szeged, Dóm tér 9, Szeged 6720, Hungary

⁴ELI-ALPS, ELI-HU Non-Profit Ltd., Dugonics ter 13, Szeged 6720, Hungary

⁵Physics Department, Technische Universität München, James-Frank-Str. 1, 85748, Garching, Germany

⁶Department of Applied Physics, The Hebrew University of Jerusalem, Jerusalem, 91904, Israel

⁷FORTH-IESL, PO Box 1527, GR-711 10 Heraklion, Crete, Greece

⁸Department of Physics, University of Crete, PO Box 2208, GR71003 Heraklion, Crete, Greece

⁹National Institute for R&D of Isotopic and Molecular Technologies, Donath 67-103, 400293 Cluj-Napoca, Romania

¹⁰Department of Physics, Umeå University, SE-901 87 Umeå, Sweden

¹¹Current address: European XFEL GmbH, Holzkoppel 4, 22869 Schenefeld, Germany

¹²e-mail: daniel.rivas@xfel.eu

[†]These authors contributed equally for this work.

*Corresponding author: laszlo.veisz@umu.se

Published 12 October 2018

This document provides supplementary information to “Propagation-enhanced generation of intense high-harmonic continua in the 100-eV spectral region,” <https://doi.org/10.1364/OPTICA.5.001283>. The document includes additional single-shot images of high-harmonic spectra measured under different generation conditions, additional information on the intensity measurement and calculation as well as the theoretical model, and finally results on the single-atom response and macroscopic harmonic intensity calculated from the model.

1. ADDITIONAL SINGLE SHOT IMAGES OF THE SPATIO-SPECTRAL ENERGY DENSITY DISTRIBUTION

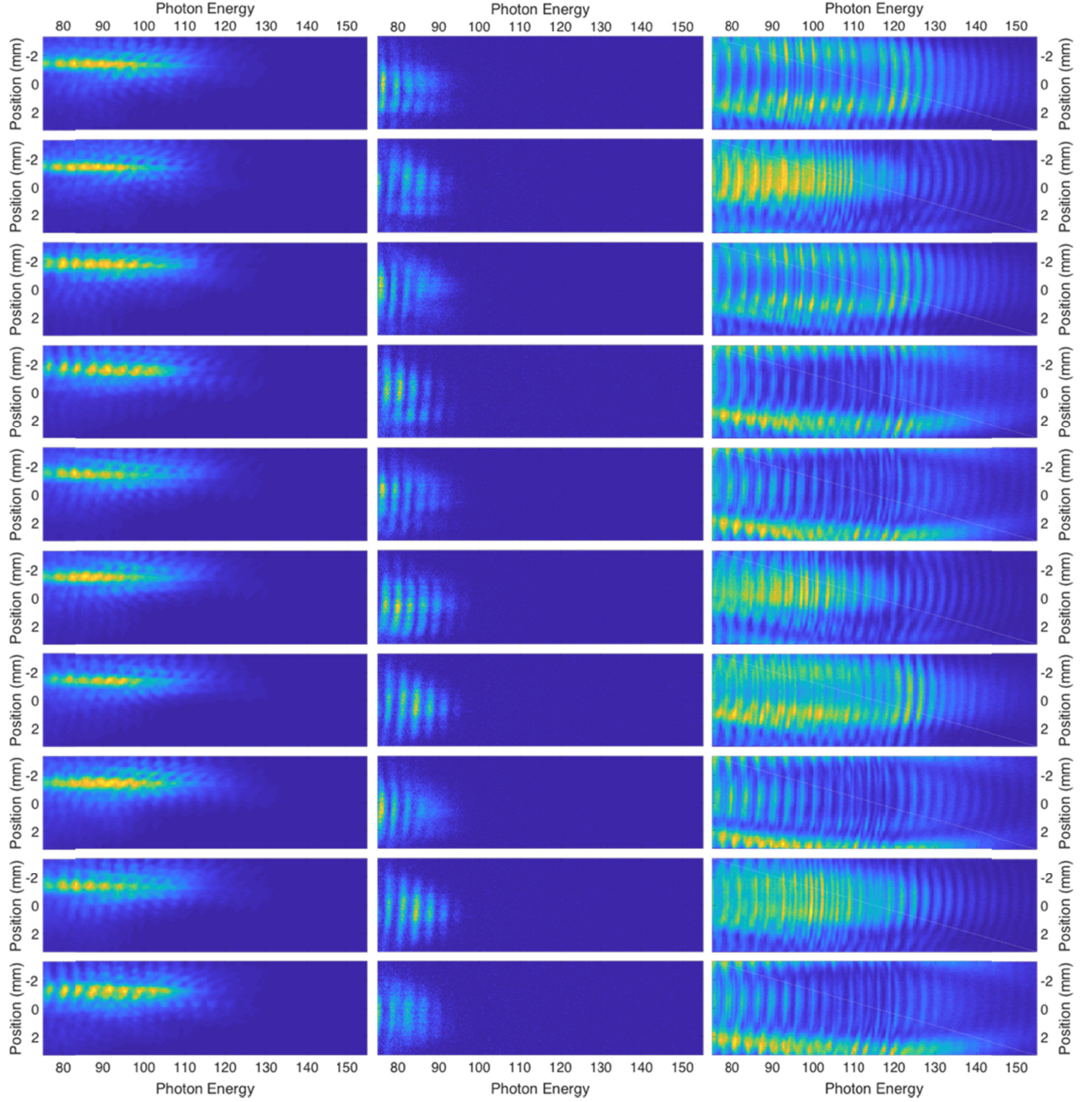


Fig. S1. Ten different single-shot images of the spatio-spectral energy density distribution for the 10 cm cell at optimized conditions (left column), for the 10 cm cell at an intensity of $5 \times 10^{14} \text{ W/cm}^2$ (middle column) and the 1.5 mm nozzle at optimized conditions (right column). The shots were selected from larger data sets, and were acquired under otherwise similar experimental conditions. The images depict the differences between the three regimes: stable and showing relatively weak spectral modulations (left column), shot-to-shot changes at the cutoff-energy region between 85-95 eV (middle column), and strong shot-to-shot changes in spatio-spectral intensity distribution in (right column). As mentioned in the main text, the fluctuations seen in the middle and right columns are attributed to the random-varying value of the CEP.

2. ON-TARGET INTENSITY MEASUREMENT AND CALCULATION

The beam profile at the target plane and the corresponding pulse energy are measured in single-shot. A beam size of approximately 360 μm FWHM and a pulse energy of about 40 mJ is obtained on average. Separately, the pulse duration is measured on target through the chirp-scan technique [1, 2], with a value of approximately 4.5 fs. With this characterization we estimate an on target intensity of $1\text{-}2 \times 10^{15} \text{ W/cm}^2$.

For the simulations, the focusing geometry and laser beam parameters are adjusted to match the measured intensity distribution. The calculation of the laser beam propagation is done through the ABCD-Bessel (or ABCD-Hankel) transform, based on the Fresnel diffraction integral [3]. At the starting plane, we assume an 8th order super-Gaussian spatial intensity distribution with a size of 50 mm FWHM. In accordance with the experimental setup, the beam is clipped by a hard aperture of 45 mm in diameter and then propagates 20 m to the focusing optic. To account for the unknown beam size, divergence and beam imperfections at the focusing optic (due to the use of an adaptive mirror before entering the vacuum beam-delivery line) a focal length of 22.5 m (instead of 17 m) is used in the simulation. This is equivalent to varying the effective f-number in order to match the measured beam size at the focal plane (360 μm). Finally, to match the measured instantaneous intensity the pulse energy was set to 21 mJ, the temporal duration to 4.5 fs (FWHM) and the central wavelength to 800 nm. The pulse energy used in the simulations is lowered in order to account for the reduced energy due to beam reduction by a hard aperture and to imperfect focusing in the experiments. Although, some energy is located outside the focal spot, due to the lower intensity it does not influence the XUV field during HHG.

3. THEORETICAL MODEL

The simulations were carried out using a three-dimensional non-adiabatic simulation code which was first introduced in [4], which has since then been extensively developed [5], including the treatment of high intensity laser propagation when multiply ionized species of the atomic gas are also generated [6]. After calculating the spatio-temporal distribution of the electric field at the entrance of the interaction region, the code simulates HHG in the following three main steps. First, the propagation of the generating laser field (E_1) is calculated based on the wave equation of the form [7]:

$$\nabla^2 E_1(r, z, t) - \frac{1}{c^2} \frac{\partial^2 E_1(r, z, t)}{\partial t^2} = \frac{\omega^2}{c^2} (1 - \eta_{\text{eff}}^2) E_1(r, z, t) \quad (\text{S1})$$

The above expression can be simplified using paraxial approximation and moving temporal frame (with speed of light c). The actual equation that is solved in Fourier space (applying the Crank-Nicolson method) is

$$\left(\frac{\partial^2}{\partial r^2} + \frac{1}{r} \frac{\partial}{\partial r} \right) E_1(r, z, \omega) - \frac{2i\omega}{c} \frac{\partial E_1(r, z, \omega)}{\partial z} = \frac{\omega^2}{c^2} \hat{F} \left[(1 - \eta_{\text{eff}}^2) E_1(r, z, t) \right] \quad (\text{S2})$$

where \hat{F} is the Fourier operator. In the spatial and temporal variation of the refractive index $\eta_{\text{eff}}(r, z, t)$ the dispersion of atoms, the optical Kerr-effect and the plasma dispersion is included.

Having the temporal variation of the laser field in all the discretized spatial points of the simulated volume the second step is to calculate the nonlinear polarization of the gas medium. The single-dipole response is obtained using the strong-field approximation, that is by using the Lewenstein integral [8], taking into account the depletion of the initial state due to ionization (described by ionization rate $w(t)$) and using the saddle-point solution for the momentum p_{st} and action S_{st} (with respect to momentum) [9]:

$$\begin{aligned} x_{\text{nl}}(t) = 2 \text{Re} \left\{ i \int_{-\infty}^t dt' \left(\frac{\pi}{\epsilon + i(t-t')/2} \right)^{\frac{3}{2}} d^* [p_{st}(t', t) - A_1(t)] \right. \\ \left. \times E_1(t') \cdot \exp[-iS_{st}(t', t)] \cdot d[p_{st}(t', t) - A_1(t')] \right\} \\ \times \exp \left[- \int_{-\infty}^t w(t') dt' \right] \end{aligned} \quad (\text{S3})$$

The dipole matrix element d is assumed to be hydrogen-like [4,8].

The last step is to solve the same type of equation as Eq. S1, but for the harmonic field E_h . The source term is the time-dependent macroscopic dipole P_{nl} of the medium obtained from the single-dipole response x_{nl} , taking into account the ionization probability and the gas density (similarly to how it is done in Ref. [10]):

$$\nabla^2 E_h(r, z, t) - \frac{1}{c^2} \frac{\partial^2 E_h(r, z, t)}{\partial t^2} = \mu_0 \frac{\partial^2 P_{\text{nl}}(r, z, t)}{\partial t^2} \quad (\text{S4})$$

The interaction region (both for the cell and jet) was assumed to have a constant pressure distribution (6.7 mbar and 240 mbar for the cells and jet, respectively). The gas targets were placed 10 cm before the geometrical focal plane, matching the experimental situation. From the end of the interaction region the generated radiation was propagated a distance of 12 m (using again the ABCD-Bessel transform [3]), which approximately corresponds to the detection plane in the experiments.

For the calculation of the spatio-temporal intensity of the high-harmonic radiation the theoretical amplitude and phase of the optical elements (filter and dielectric mirror) were taken into account.

4. SINGLE ATOM RESPONSE AND HARMONIC INTENSITY

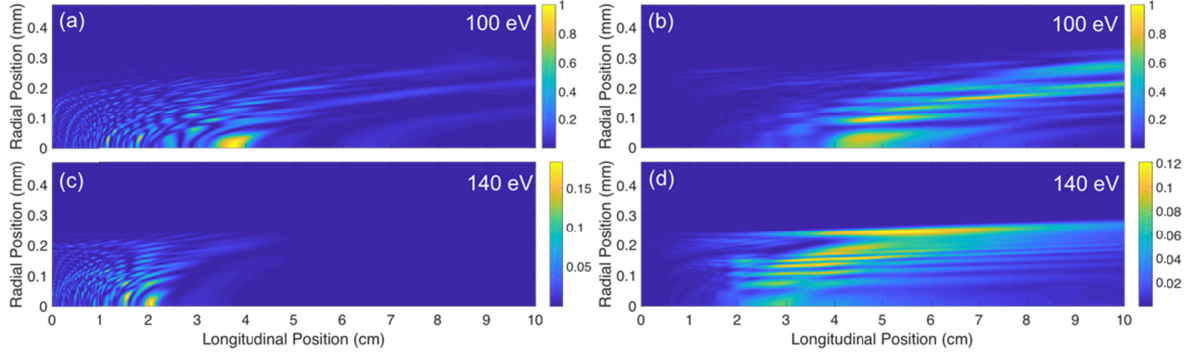


Fig. S2. Calculated spatial distribution of the single-atom response inside the 10-cm gas cell for a photon energy of (a) 100 eV and (c) 140 eV. For both cases, the single-atom response peaks before the steady region. The corresponding macroscopic harmonic intensity (b), and (d) have their optimum in the steady region. At 140 eV the overall emission is reduced towards the end of the cell due to phase mismatch and reabsorption. This explains why radiation above 130 eV is not observed, despite the semi-classical model predicting a cutoff energy of 155 eV. Additionally, we emphasize that these plots show the radiation in a plane, whereas the measured radiation is projected. This means that the off-axis contributions are scaled with the radius, so for the 100 eV harmonic the flux at the output of the 10 cm cell is similar in magnitude as the 5 cm cell output.

References

1. Lorient, V., Gitzinger, G. & Forget, N. "Self-referenced characterization of femtosecond laser pulses by chirp scan", *Optics Express* 21, 24879–24893 (2013).
2. D. E. Rivas et al. "Next generation driver for attosecond and laser-plasma physics", *Scientific Reports* 7, 5224 (2017).
3. Z. Zalevsky, Z. et al., "The ABCD-Bessel transformation", *Optics Communications* 147, 39-41 (1998).
4. E. Priori et al., "Nonadiabatic three-dimensional model of high-order harmonic generation in the few-optical-cycle regime", *Physical Review A* 61, 063801 (2000).
5. V. Tosa et al., "Macroscopic generation of attosecond-pulse trains in strongly ionized media", *Physical Review A* 79, 043828 (2009).
6. V. Tosa et al., "Propagation effects in highly ionised gas media", *Quantum Electronics* 46, 321 (2016).
7. E. Esarey et al., "Self-focusing and guiding of short laser pulses in ionizing gases and plasmas", *IEEE Journal of Quantum Electronics* 33, 1879-1914 (1997).
8. M. Lewenstein et al., "Theory of high-harmonic generation by low-frequency laser fields", *Physical Review A* 49, 2117-2132 (1994).
9. G. Sansone et al., "Nonadiabatic quantum path analysis of high-order harmonic generation: Role of the carrier-envelope phase on short and long paths", *Physical Review A* 70, 013411 (2004).
10. M. B. Gaarde et al., "Macroscopic aspects of attosecond pulse generation". *Journal of Physics B* 41, 132001 (2008).